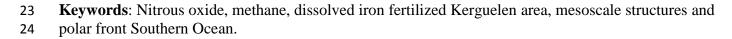
1	Dissolved greenhouse gases (nitrous oxide and methane) associated with the naturally iron-
2	fertilized Kerguelen region (KEOPS 2 cruise) in the Southern Ocean
3	
4	L. Farías ¹ *, L. Florez-Leiva ² , V. Besoain ^{1,3} , G. Sarthou ⁴ , and C. Fernández ⁵
5	
6 7	¹ Departamento de Oceanografía. Universidad of Concepción and Centro de Ciencia del Clima y la Resiliencia (CR) ² , Chile
8	
9	² Programa de Biología. Universidad del Magdalena, Santa Marta, Colombia
10	
11	³ Escuela de Ciencias del Mar, Pontificia Universidad Católica de Valparaíso, Chile
12	⁴ LEMAR-UMR 6539, CNRS-UBO-IRD-IFREMER, Place Nicolas Copernic, 29280 Plouzané, France
13 14 15 16	⁵ Sorbonne Universités, UPMC Univ Paris 06, UMR 7621, Laboratoire d'Océanographie Microbienne, Observatoire Océanologique, F-66650 Banyuls/mer, France and Department of Oceanography, COPAS SA program and Interdisciplinary Center for Aquaculture Research (INCAR), University of Concepción, Chile
17	
18	
19	Correspondence should be addressed to:
20	Laura Farias; lfarias @profc.udec.cl
21	
22	
23	
24	
25	
26	

1

2 ABSTRACT

3 The concentrations of greenhouse gases (GHGs) like nitrous oxide (N_2O) and methane (CH₄) were 4 measured in the Kerguelen Plateau Region (KPR), an area with an annual microalgal bloom caused by natural Fe fertilization, which may stimulate microbes involved in GHG cycling. This study was carried 5 6 out during the KEOPS 2 cruise during the austral spring of 2011. Oceanographic variables including N₂O and CH₄ (from surface to 500 m depth) were sampled in two transects along and across the KRP, 7 the north-south (N-S) transect (46°-51°S, ~72°E) and the west-east (W-E) transect (66°-75°E, ~48.3°S 8 9); both associated with the presence of a plateau, polar fronts and other mesoscale features. The W-E 10 transect had N_2O levels ranging from equilibrium (105%) to slight supersaturation (120%) with respect to the atmosphere. CH₄ levels fluctuated dramatically, with high supersaturations (120-970%) in areas 11 close to the coastal waters of Kerguelen Island and in the polar front (PF). The N-S transect showed a 12 more homogenous distribution for both gases, with N₂O and CH₄ levels from 88% to 171% and 45% to 13 666% saturation, respectively, but surface CH_4 peaked at southeastern stations of the KPR (A3 stations), 14 15 where a phytoplankton bloom was observed. Both gases responded significantly, but in contrasting ways (CH₄ accumulation and N_2O depletion), to the patchy distribution of particulate matter as 16 chlorophyll a. This seems to be strongly stimulated by Fe supply from different sources. Air-sea fluxes 17 for N₂O (from -10.5 to 8.65, mean 1.71 μ mol m⁻² d⁻¹) and for CH₄ (from 0.32 to 38.1, mean 10.07 μ mol 18 $m^{-2} d^{-1}$) indicated that the KPR is both a sink and a source for N₂O, and a considerable and variable 19 20 source for CH_4 . These results are previously unreported for the Southern Ocean and it is suggested that it may be caused by an intense microbial CH₄ production. 21

22



1 1. Introduction

The increasing concentration of greenhouse gases (GHGs) in the troposphere, such as CO₂, N₂O and CH₄, affect the Earth's radiative balance. Additionally, the increasing concentration of ozone-depleting gases (such as chlorofluorocarbons and N₂O) in the stratosphere is weakening the ozone shield, permitting higher levels of damaging ultraviolet radiation to reach the Earth's surface. The strength of each GHG is determined by its respective residence time in the atmosphere (Cicerone and Orelamland, 1988) and the magnitude of emissions to the atmosphere, of which the oceans make an important contribution (IPCC, 2007).

9 Although oceans are generally considered to be a net source of GHGs to the atmosphere, such as N_2O 10 and CH_4 , the oceanic distribution of these GHGs and the amount of exchanged via the air-sea interface 11 is highly variable (Nevison et al., 1995; Holmes et al., 2000; Rhee et al., 2009). Thus, source and sink behaviors of GHGs have been observed on different spatial and temporal scales. In general terms, these 12 13 behaviors depend on biological and physical processes that promote outgassing or sequestering mechanisms. Physical and biological features of the Southern Ocean suggest the existence of a potential 14 for both the production and removal of CH₄ and N₂O (Rees et al., 1999; Tilbrook and Karl, 1994), 15 although very little information on dissolved N₂O and CH₄ distributions is currently available for the 16 17 region. The substantial spatial variation in regional gas exchange could be due to the increased gas solubility in low-temperature Sub- and Antarctic waters, combined with either the downwelling 18 19 associated with intermediate and deep water formation over the convergence band (Antarctic Polar Frontal Zone or "PFZ"), or the low-temperature Antarctic waters, along with the upwelling of deep and 20 21 intermediate waters in the southern part of the PFZ (Parker and Viver, 2012).

In different regions of the Southern Ocean, the surface layer is always supersaturated with CH₄ (Bates et
al. 1996; Tilbrook and Karl, 1994, Toshida et al., 2011), but this is not the case for N₂O that is observed

in an under- or super saturated condition (Law and Ling, 2001, Rees et al., 1997, Zhan and Chen, 1 2 2009). Aside from physical processes affecting GHG concentrations in the water column and their 3 concomitant air-sea fluxes, they additionally depend on organic matter (OM) availability and oxygen levels, which determine whether aerobic or anaerobic OM respiration occurs (Codispoti et al., 2001; 4 5 Reeburgh, 2007). The availability of dissolved iron (dFe) should also be included as a variable affecting 6 GHG cycling; directly as several Fe-containing enzymes, which are involved in the electron transfer chains in bacterial respiratory systems and Nitrogen cycling, are required for GHG cycling (Arrieta et al, 7 2004; Kirchman et al., 2003; Morel et al., 2003a) and, indirectly as dFe stimulates ocean productivity 8 9 which can enhance carbon and nitrogen export from the euphotic zone to the subsurface (Boyd and Ellwood, 2010), resulting in a an increase of the microbial activities which may mediate GHG via 10 nitrification (Fuhrman and Capone, 1991), 11

 N_2O is mainly produced during the first step of nitrification; the aerobic oxidation of NH_4^+ to NO_2^- and 12 during partial denitrification, the anaerobic reduction of NO₃⁻/NO₂⁻ to N₂O. N₂O can also be consumed 13 by complete denitrification via dessimilatory reduction to N₂ (Codispoti and Cristiensen, 1985) or 14 assimilatory N₂O reduction to NH₄⁺ (Farias et al 2013). CH₄, on the other hand, is mainly formed by 15 methanogens during anaerobic OM degradation (Wuebble & Hayboe, 2001) or by methylotrophs during 16 17 CH₄ formation derived from transformations of methyl-compounds such as methylphosphonate (MPn) (Karl et al., 2008), dimethyl-sulphoniopropionate (DMSP) (Damm et al., 2010) and dimethylsulphide 18 (DMS) (Florez-Leiva et al., 2013). In addition, CH₄ can be consumed (oxidized) via aerobic 19 20 methanothophy (Hanson and Hanson, 1996). Since Southern Ocean waters are well oxygenated, N_2O formed by nitrification (Nevison et al., 2003) and CH_4 formed by either methanogenesis in suspended 21 particles (Scranton and Brewer 1977) or by methylotrophy, are thought to be the dominant mechanisms 22 23 of production in surface waters (Sun et al., 2011).

1 The main objective of the present study is to describe for first time the N₂O and CH₄ contents in the 2 Southern Ocean under the influence of natural fertilization events during the spring phytoplankton bloom in the KPR. The determination of the role of the Southern Ocean in CH₄ and N₂O air-sea 3 exchange may be critical in understanding the factors/variables that influence GHG cycling. This 4 includes dFe which comes from different sources within the KPR, inducing mesotrophic conditions that 5 6 are associated with the coastal waters of Kerguelen Island, the area of quasi permanent phytoplanktonic bloom in the Central Plateau area of the KPR(Blain et al., 2008; Chever et al., 2010), and with the 7 Antarctic Polar front and other mesoscale structures (Mongin et al., 2008, Lasbleiz et al., 2014). 8

9 2. Methods

10 **2.1. Study area**

Samples were collected within the Kerguelen Plateau Region or KPR (Fig. 1) during the KEOPS 2 11 cruise at stations along north to south (TNS,46°-51°S) and west to east (TWE, 66-75°E)transects. The 12 cruise was carried out from October 11th to December 11th, 2011, on board the research vessel (RV) 13 Marion-Dufresne. Some of the sample stations were located in the PFZ in the coastal shelf waters of 14 Kerguelen Island and within the southeastern KPR bloom (including station A3 from the previous 15 KEOPS 1 cruise), which are naturally Fe-enriched, however another station was sampled (St. R), which 16 17 is located beyond the KPR and considered to be representative of the HNLC area off the KPR (see Table 1). The hydrographic condition of the sampling stations was selected according to a strategy based on 18 real-time ocean color and altimetry satellite images (d'Ovidio et al., 2012). 19

20 2.2. Continuous and discrete sampling: Continuous vertical profiles of temperature, salinity, dissolved
O₂, fluorescence and photosynthetically active radiation (PAR) were obtained using a conductivity
temperature and depth (CTD) sensor. Water was sampled with a CTD-Rosette sampler (SBE 32 24x10L Carousel Water Sampler with 10-L Niskin bottles). Water samples for gases (N₂O, CH₄), nutrients,

1 and pigments (sampled in this correlative order) were obtained from nine depths distributed between the 2 surface and a 500m depth. Water samples for CH_4 (triplicate) and N_2O (triplicate) analyses were taken in 3 20 mL glass vials and poisoned with $HgCl_2$ (0.1 ml of saturated $HgCl_2$ solution per vial). The vials were then sealed with a butyl-rubber septum and aluminum cap, avoiding bubble formation, and stored at 4 room temperature in darkness until laboratory analysis. Syringes of 50 mL were directly connected to 5 the spigot of the Niskin bottles to take nutrient samples (NO_3, NO_2, PO_4^3) and Si $(OH)_4$ at each 6 sampled depth. Duplicate samples were collected and drawn through a 0.45 µm Uptidisc adapted to the 7 syringe, and then immediately analyzed using an autoanalyzer (more details in Blain et al, this volume). 8 9 Total chlorophyll-a (*TChl-a*) samples in triplicate were filtered into a 25 mm glass- fiber filter (GF/F), and then immediately frozen (-20°C). Samples were kept until later analysis by high performance liquid 10 chromatography (HPLC) (more details in Lasbleiz et al., 2014). 11 **2.3.** Chemical analysis: N_2O and CH_4 were analyzed by creating into the vial 5 mL of ultra-pure 12 Helium headspace throughout a gastight syringe, followed by an equilibration of gas and liquid phase in 13 the vial at 40° C, and then quantifying gases by a gas chromatograph determined by helium (He) 14 equilibration (5-mL helium headspace and 15-mL of seawater) at 40°C in the vial, followed by 15 quantification via chromatography. N₂O was analyzed in a Varian 3380 Gas Chromatograph using an 16 17 electron capture detector at 350°C and connected to an autosampler device. CH₄ was analyzed in a Schimadzu 17A gas chromatograph using a flame ionization detector at 250°C through a capillary 18 column GS-Q at an oven temperature of 30° C. A calibration curve was made with four concentrations 19 20 for N₂O (0.1 ppm, 0.32, 0.5 ppm, and 1 ppm, by Matheson standards) and four concentrations for CH_4 (0.5, 1.78, 2 and 10 ppm, by Matheson standards). Both detectors linearly responded to these 21 concentration ranges. The analytical error for the N₂O and CH₄ analyses was less than 3% and 5% 22

- respectively. The samples were taken in triplicate in 20 mL vials and carefully sealed to avoid air

bubbles. They were then preserved with 50 µL of saturated HgCl₂ and stored in darkness until analysis.
The ECD and FID detectors lineally responded to these concentration ranges and the analytical error
for the N₂O measurements for this study was about 3%. The uncertainty of the measurements was
calculated from the standard deviation of the triplicate measurements by depth. Samples with a variation
coefficient higher than 10 % were not taken into account for the gas database.

More details regarding the analysis of both gases can be found in Farias et al. (2009). Nutrients were
immediately analyzed onboard by standard automated colorimetric methods (Tréguer and LeCorre,
1975) using the continuous flow autoanalyser (Skalar). The precision and detection limit of the method
was, respectively, ±50 nM and 20 nM for NO3-, and ±30 nM and 110 nM for PO₄⁻ (more details in Blain
et al. this volume). NH4+ was measured by fluorometric analysis (Holmes et al., 2000) with a precision
of ±50 nM.

2.4. Data analysis: To interpret the vertical variation of N₂O and CH₄ and how biogeochemical 12 13 processes may affect their concentrations, the water column was divided into two layers according to density gradient: (1) well-mixed and (2) subsurface from the base of the mixed layer (ML) to 500 m 14 (arbitrary depth used only for comparison proposes). Nutrient inventories for T*Chl-a*, N₂O and CH₄ 15 were calculated by numerical integration of data at one meter (linear interpolation) increments based on 16 17 at least 4-6 sampled depths per layer. Saturation percentages of gases were calculated from the measured CH₄ and N₂O concentrations and those estimated to be in equilibrium with the current gas concentrations 18 in the atmosphere (NOAA register (http://www.esrl.noaa.gov/gmd/hats/combined /N₂O.html), based on 19 *in situ* temperature and salinity according to the solubility parameterization CH₄ (Wiesenburg and 20 21 Guinasso, 1979) and N_2O (Weiss and Price, 1980). GHG flux through the air-sea interface was 22 determined using the following equation, modified by Wanninkhof (1992):

$$F = kw(T^{\circ}, salinity) \cdot (C_w - C_a)$$

1	where kw is the transfer velocity from the ML to the atmosphere, as a function wind speed, temperature
2	and salinity in the ML according to parametrization, C_w is the mean gas concentration in the mixed
3	layer, while C _a is the gas concentration in the mixed layer expected to be in equilibrium with the
4	atmosphere. Since gas transfer velocity is related to wind speed, this was calculated according to the
5	well-known exchange models of Liss and Merlivat (1986) or LM86 and Wanninkhof (1992) or W92,
6	based on the dependence of the transfer velocity on wind speed. Wind speed and direction were obtained
7	from an onboard register using the ship's meteorological station as per international protocols. Wind
8	speed was estimated as a moving average of seven days before the sampling (stations) in order to
9	smooth out short-term fluctuations and highlight longer-term trends. The mixed layer depth was
10	calculated using a potential density-based criterion, defining the mixed layer depth (ML) as the
11	shallowest depth at which density increased by 0.02 kg m^{-3} from the sea surface value.
12	Pearson product-moment correlations (rs) were determined for GHG, and TChl-a and nutrient
13	inventories were estimated in the ML and in the whole water column from surface to 500 m depth. The
14	threshold value for statistical significance was set as p <0.05. A principal component analysis (PCA)
15	using the empirical orthogonal function (EOF; Emery and Thomson, 1997) was performed to find the
16	co-variability patterns of a number of stations located in spatial gradients in terms of nutrients, gases
17	(O ₂ , N ₂ O, and CH ₄), T <i>Chl-a</i> , and dFe. This analysis excluded the stations from the NS transect as no
18	measurements were recorded (Quéroué et al, this volume). PCA were made with all biogeochemical
19	variables measured in the ML and with these variables obtained in the water column from the surface to
20	a depth of 500 m, in order to discern differences in the vertical structure.

Results

3.1. Oceanographic conditions.

Oceanographic characteristics of the sampled stations during the KEOPS 2 cruise are shown in Table 1.
 Two transects, almost synoptically made across and along the KPR (survey region – Fig. 1) were
 undertaken to establish the position of the main mesoscale structures as fronts (Figure 2). The Polar
 Front (PF) crosses the KPR and demarcates certain physical structures (convergence process) visible
 throughout temperature and salinity.

Regarding the W-E transect or TWE (66° to 75°E, along 47°S, Fig. 2 a,c,e), vertical cross sections of 6 temperature and salinity with a T-S diagram are illustrated in Fig 2 (a,c,e). Temperature and salinity 7 varied between 2.41° and 3.3°C, and between 33.60 and 34.67, respectively. A weak structure with 8 9 colder and fresher surface waters was registered in the FP, which crossed these transects twice, at \sim 71°E (St. TWE03-04) and at ~73.5°E (StTWE07-08). Middle stations (Sts. TWE04, -05 and E) denoted an 10 area with a complex recirculatory system in a stationary meander of the PF (Park et al., 2014), hereafter 11 known as the Central Section. This section is superficial bathed by mixed Antarctic surface water 12 (AASW) and coincides with the area with the PF northward inflexion (Fig. 1). The presence of 13 Subantarctic mode water (SAMW) was observed east of 73.5° E (Sts. TWE07-08, Fig. 2f). In addition, a 14 marked variability in subsurface water was observed, ascribed to mixing water masses; this was 15 particularly strong in TWE within the PF, revealing a vertical mixing process produced by convergence, 16 17 particularly evident at St. TWEO7 (Fig. 2e). Regarding the N-S transect (46° -51°S, along ~72°E) or TNS, Fig. 2 (b, d, f) shows vertical cross sections of temperature, salinity and a T-S diagram, 18 respectively. Temperature and salinity fluctuated from 1.67° to 4.17°C and from 33.67 to 34.68, 19 20 respectively, and a gradual decrease in temperature and an increase in salinity were observed in the surface layer from north to south (Fig 2 b, d). There was a water parcel of a relatively colder water mass 21 spreading northward in subsurface waters. This was an expression of the PF, which marked the location 22 23 where the AASW moving northward descended rapidly and sank below a depth of 200 m depth (Fig. 2

b). These distributions coincided with the expected water mass distribution, this being the case for the
northern (Sts. TNS01-02) and southern (Sts. A3, TNS10) stations, mainly occupied from the surface to
250 m by the SAMW and the AASW, respectively (Fig 2f).

4 **3.2.** Biogeochemical variables

5 Figure 3 shows vertical cross sections along the TWE of biogeochemical variables including nutrients

6 (only NO_3^- and $HPO_4^{2^-}$), T*Chl-a*, O_2 and GHGs. The surface layer continuously showed NO_3^-

7 concentrations, fluctuating from 22 to 27 μ mol L⁻¹ (typical condition of the AASW). However, a relative

depletion of NO_3^- was observed at the stations located north- and eastward of the PF (Fig 3a). PO_4^{3-}

9 presented the same pattern as NO_3^- and the N:P ratio of dissolved nutrients averaged around 14.5, with

10 the exception of some values of 13.2 from stations located closed to the PF (Fig. 3 b). *TChl-a* fluctuated

from 0.005 to 4.69 μ g L⁻¹ and peaked at Sts. TWE01-02 (both located in a coastal area 10 and 75 km

12 away from Hillsborough Bay coast) and Sts. TWE07-08 (to the north of PF). *TChl-a* showed a relative

decrease at stations located in the Central Section (Fig. 3c). The observed pattern (Lasbleiz et al., 2014)

significantly correlated with the dFe spatial distribution reported by Quéroué et al. (this volume). O₂

15 concentration varied form 320 μ M (in surface water) to 185 μ M (at 500 m deph), consistently

16 maintaining super saturation conditions (Fig 3d).

17 N₂O fluctuated from 14.0 to 25.4 nmol L^{-1} (equivalent to a range of 102-182.2% saturation, Fig 3e).

18 Superficially, the N₂O concentration was close to equilibrium with the atmosphere in surface waters in

19 the western and central section (70.5°- 73°E) and slightly undersaturated (around 90%) in surface waters

20 in sites where the PF crosses the transect, i.e., Sts. TWE04 and TWE07 (Fig. 3e). N₂O levels

21 increased slightly attaining around 120% saturation towards subsurface water. CH₄ ranged from 1.4 to

22 31.35 nmol L^{-1} , equivalent to a range of saturation of 43-969%. In contrast to N₂O, surface waters were

always supersaturated in CH₄, showing the highest increase in gas levels (up to 970%) in coastal waters

1	close to Kerguelen Island, a relative decrease (<200% saturation) in the central section (between 71° and
2	73.5°S, or Sts TWE04, 05 and E2), and a strong increase (up to 778%) at St, TWE07. Remarkably, CH_4
3	concentrations in subsurface waters were low compared to the surface waters (Fig. 3f).
4	Vertical cross sections of biogeochemical variables along the TNS are shown in Figure 4. NO_3^- and
5	PO_3^{4-} gradually increased from north to south from 24 to 30 µmol L ⁻¹ and from 1.5 to 2 µmol L ⁻¹ ,
6	respectively (Fig 4 a, b). This spatial trend coincided with the expected transition of water mass
7	dominance and its mixing between the SAMW and the AASW (Fig 2 f). TChl-a ranged from 0.005 to
8	2.391 μ g L ⁻¹ and peaked in the southernmost stations (Sts. TNS08, -09 and A3-2; Fig. 4b) and coincided
9	with a slight increase in nutrients. These trends coincided with the presence of the central plateau area of
10	the KPR, where upwelling-like circulation was observed (Zhou, this volume), as indicated by
11	temperature and salinity distribution (Fig. 2 b, d). There a deep Fe-enriched and lithogenic silica
12	reservoir seems to be influencing the area (Lasbleiz et al., 2014; Quéroué et al., 2014). O ₂ distribution
13	was similar to that observed in the WE transect.
	was similar to that observed in the WE transect. N ₂ O concentrations ranged from 12.37 to 23.8 nmol L^{-1} , equivalent to 88.5% to 171% saturation. N ₂ O
13	
13 14	N_2O concentrations ranged from 12.37 to 23.8 nmol L ⁻¹ , equivalent to 88.5% to 171% saturation. N_2O
13 14 15	N_2O concentrations ranged from 12.37 to 23.8 nmol L ⁻¹ , equivalent to 88.5% to 171% saturation. N_2O levels close to equilibrium or undersaturation were often observed in surface waters, except at St.
13 14 15 16	N_2O concentrations ranged from 12.37 to 23.8 nmol L ⁻¹ , equivalent to 88.5% to 171% saturation. N_2O levels close to equilibrium or undersaturation were often observed in surface waters, except at St. TNS08 (Fig. 4e). CH ₄ varied from 1.47 to 21.88 nM, or 45 to 666% saturation, and peaked in southern
13 14 15 16 17	N_2O concentrations ranged from 12.37 to 23.8 nmol L ⁻¹ , equivalent to 88.5% to 171% saturation. N_2O levels close to equilibrium or undersaturation were often observed in surface waters, except at St. TNS08 (Fig. 4e). CH ₄ varied from 1.47 to 21.88 nM, or 45 to 666% saturation, and peaked in southern stations (Fig 4f). Notably, <i>Chl-a</i> corresponded to the observed CH ₄ in this transect. Southern stations,
13 14 15 16 17 18	N_2O concentrations ranged from 12.37 to 23.8 nmol L ⁻¹ , equivalent to 88.5% to 171% saturation. N_2O levels close to equilibrium or undersaturation were often observed in surface waters, except at St. TNS08 (Fig. 4e). CH ₄ varied from 1.47 to 21.88 nM, or 45 to 666% saturation, and peaked in southern stations (Fig 4f). Notably, <i>Chl-a</i> corresponded to the observed CH ₄ in this transect. Southern stations, such as St. A3, located in an area of relatively high bioavailable Fe and within a phytoplankton bloom,
13 14 15 16 17 18 19	N_2O concentrations ranged from 12.37 to 23.8 nmol L ⁻¹ , equivalent to 88.5% to 171% saturation. N_2O levels close to equilibrium or undersaturation were often observed in surface waters, except at St. TNS08 (Fig. 4e). CH ₄ varied from 1.47 to 21.88 nM, or 45 to 666% saturation, and peaked in southern stations (Fig 4f). Notably, <i>Chl-a</i> corresponded to the observed CH ₄ in this transect. Southern stations, such as St. A3, located in an area of relatively high bioavailable Fe and within a phytoplankton bloom, had extremely low N ₂ O concentrations (less than 6.9 nM or 70% saturation).
13 14 15 16 17 18 19 20	N ₂ O concentrations ranged from 12.37 to 23.8 nmol L ⁻¹ , equivalent to 88.5% to 171% saturation. N ₂ O levels close to equilibrium or undersaturation were often observed in surface waters, except at St. TNS08 (Fig. 4e). CH ₄ varied from 1.47 to 21.88 nM, or 45 to 666% saturation, and peaked in southern stations (Fig 4f). Notably, <i>Chl-a</i> corresponded to the observed CH ₄ in this transect. Southern stations, such as St. A3, located in an area of relatively high bioavailable Fe and within a phytoplankton bloom, had extremely low N ₂ O concentrations (less than 6.9 nM or 70% saturation). PCA, including dFe and GHG data were obtained from the TWE as shown in Figure 5. The results did

the western or coastal area (TWE01-02), and Central section (Sts. TWE04, -05,E2). The variability among stations can be predominantly explained by the first component, accounting for 75.7% of the variance. Figure 5 demonstrates possible interpretations for relationships among the variables with their respective weights assigned to each of them (illustrated with an eigenvector). The figure shows a close relationship between N₂O, nutrients, CH₄, Fe and *Chl-a*. The PCA analysis using data from the entire water column provided a similar grouping of the sample stations (Fig 5b).

7 **3.3.** Vertical distribution of gases and other variables at selected stations

8 Figure 6 shows typical profiles of oceanographic and biogeochemical variables (including gases).

9 Stations were separated *a priori* according to biogeochemical (PCA analysis for the case of the TWE; Fig.5) and oceanographic criteria (T-S diagram, Fig. 2e, f). Selected stations included: Sts. A3, with a 10 quasi-permanent phytoplankton bloom (historical station sampled in KEOPS 1, Blain et al., 2007) and, 11 low Fe levels (~ 0.18 nmol L^{-1}), but with the evidence n of an active uptake of dFe uptake; St. TWE07, 12 which had moderate dFe (~0.40 nmol L-1) and high TChl-a levels and also evidences of rapid dFe 13 uptake (Fourquez et. this volume). For comparative purpose, we include the most northern station of the 14 NST (St. TNS01), a well-known as a Fe-limited HNLC area (St. R), and a coastal station close to 15 Kerguelen Island, which had the highest dFe levels (up to 3.82 nmol L^{-1} . Vertical distribution of N₂O 16 17 and CH_4 differed markedly, while elevated CH_4 concentrations were mostly located superficially and in the ML base and decreased as depth increased, N₂O concentrations gradually increased with depth. Gas 18 contents also differed between stations and were in similarly correlated with Chl-a and dFe levels. 19 20 Stations located in the extreme point of the WET (i.e., TWE01 and TWE07) had the highest CH_4 levels (Fig 6), while N_2O levels were relatively low. On the other hand, Sts. TNS1 and A3, located in the 21 extreme north and south of the N-S transect presented relatively low levels of CH₄ compared to the WE 22 23 transect. Station R, which is located in one of the more oligotrophic conditions of the Southern Ocean

1	(special volume of KEOPS 1), had the lowest N ₂ O and CH ₄ content, and both gases were

- 2 homogeneously distributed with depth (Fig. 6). This is consistent with the expected trophic condition
- 3 with T*Chl-a* levels of less than 0.5 μ g L⁻¹.

4 **3.4.** Nutrient, T*Chl-a*, dFe and GHG inventories and air-sea GHG exchanges

5 Table 2 shows the inventories of NO_3 , PO_4^{3-} and GHGs in the ML and the water column from the

6 surface to 500 m; mean GHG concentrations in the ML, wind speed and air-sea GHG fluxes are also

- 7 included. ML depths varied widely from 16 m (at the station near Kerguelen Island) to 181 m. The
- 8 T*Chl-a* pool, estimated on the basis of the photic layer, fluctuated from 8.77 to 75.45 mg m⁻². It was
- 9 notably greater at Sts. SPF and A3-2 (up to fivefold greater) than at more oligotrophic stations like St. R.

10 Surface NO_3^- and PO_4^{3-} inventories, which varied from 1.56 to 16.03 and 0.13 to 1.07 mol m⁻²,

11 respectively, did not show significant differences among stations. Minimal values were registered at

12 stations St. TWE07-08 and TNS01, both located north of the PF.

13 N₂O pools varied from 0.201 to 2.55 and from 1.12 to 10.05 mmol m^{-2} in the ML and whole water

column, respectively. Minimum values were registered in the ML at stations within or north of the PF.

15 These surface pools did not significantly correlate with TChl-a, but correlated strongly and negatively

with nutrients (rs: 0.91 p<0.001 for NO₃⁻ and rs: 0.92, p<0.001 for PO₄³⁻). CH₄ inventories fluctuated

between 0.19 and 3.31 mmol m^{-2} for the ML and 1.06 and 7.44 mmol m^{-2} for the WC. Once again,

inventories in the ML were two and fivefold higher at Sts. TWE07 and A3-2, respectively, than at St. R.
CH₄ inventories were four and sevenfold higher in Sts. TWE07 and A3-2 than at St. R. The comparison

20 between the CH₄ inventories standardized by the thickness of the layer), obtained from the ML and from

the entire water column, indicate that the maximum values came from the ML's base, remarkably in the

PF (Table 2). CH₄ pools correlated positively with T*Chl-a* pools (rs= 0.69; p<0.05), but did not show

1 any correlation with NO₃- and PO₄³⁻. Thus, minimum values for both nutrients were found when T*Chl-a* 2 was higher.

3	Average hourly wind velocity during the cruise was 10.53 ± 5.52 m s ⁻¹ , occasionally falling below 0.31
4	m s ^{-1} or rising above 29.1 m s ^{-1} . The ML depth did not show any significant relationship to wind speed
5	(rs: 0.20 p=0.41) or the water mass structure (Table 1 and Fig. 2), but seems to be related to the complex
6	mesoscale circulation observed in the KPR (Park et al., 2014; Zhou et al. this volume). N ₂ O fluxes,
7	estimated by LM86, fluctuated between -9.69 and 10.02 (mean: $1.25\pm4.04 \mu mol m^{-2} d^{-1}$), while those
8	estimated by W92 varied from -18.69 to 20.2 μ mol m ⁻² d ⁻¹ (mean: 2.41 \pm 7.88). At high wind speeds,
9	such as those measured during the N-S transect (21-23 October 2011, mean value of 12.08 m s ^{-1})
10	compared to those registered during the W-E transect (31 October – 02 November, mean value of 5.61
11	m s $^{-1}$), substantial differences were observed between the cubic (LM86) and the quadratic
12	parameterizations (W92). The latter increased in calculated fluxes by approximately a factor of two at
13	high wind speeds, while at low wind speeds the difference between LM86 and W92 was up to a factor of
14	~1.6 (see Table 2). CH ₄ fluxes varied from 0.21 to 38.1 (mean: 10.01 ± 9.97) and from 0.32 to 70.24
15	(mean: 21.27 \pm 21.07) µmol m ⁻² d ⁻¹ , when LM86 and W92 were used, respectively. The study area at
16	times acts as a source of very high CH ₄ effluxes into the atmosphere, particularly at stations St. TNS09
17	and St. A3-3, where emissions were around three times as high as those calculated for St. R. There are
18	important differences between the two parameterizations, although the same trend was obtained among
19	stations (Table 2).

20 **4. Discussion**

21 **4.1. Physical and geochemical characteristics**

1 The Antarctic Polar Front (PF) marks an important climate boundary in terms of oceanic heat and salt 2 budgets and a biogeochemical frontier with respect to GHG content and air-sea GHG fluxes (such as 3 N₂O and CH₄). The PF path exhibits considerable variability, meandering and forming eddies and rings. The location of the PF is mainly determined by the movements of deep waters and is probably strongly 4 influenced by topography and bathymetric features such as the Drake Passage and the Kerguelen Plateau 5 6 (Sandwell and Zhang, 1989; Patterson, 2005). These mesoscale structures in the study area are always associated with strong vertical and lateral mixing and advection (Park and Viver, 2012, Park et al., 2014; 7 Zhou et al, this volume) that could create fertilization mechanisms (by both Fe and nutrient like silicate), 8 9 therefore provoking *TChl-a* production which in turn is being stimulated by the addition dFe from 10 different sources (Quéroué et al. this volume). In some regions, the main Fe input is from atmospheric deposition (Jickells et al., 2005). However, this 11 was not the case in the KPR. The main sources of iron that were evidenced in the KPR, that could also 12 potentially fertilize the northern section of the plateau, were direct runoff from the Kerguelen Island, 13 glacial melting and sedimentary inputs (Quéroué et al., 2014). Actually, the water masses found at 14 stations north of the PF (e.g. TEW07) interacted more with the plateau and the shallow coastal waters of 15 Kerguelen Island, than with the water masses from the recirculation area. This theory is consistent with 16 17 the circulation data discussed by Park et al. (2014) who demonstrated that water masses are carried northwards between the island and the recirculation area and finally looped back east of the recirculation 18 19 area. 20 The origin of the bloom in the central part of the plateau possibly comes from a deep Fe-enriched reservoir which was observed also above the Kerguelen Plateau during the KEOPS1 cruise (Blain et al., 21

22 2008; Chever et al., 2010). Non reductive dissolution of resuspended sediments is a potentially

important source of dFe; at station A3, high lithogenic silice (LSi) concentrations $(1.34 \pm 0.07 \mu mol L^{-1};$

Lasbleiz et al., 2014) were observed just above the seafloor in the benthic boundary layer (BBL), also
suggesting sedimentary inputs. In fact, using Ra isotopes to trace Fe, Sanial et al. (2014) indicated that
Fe could be supplied from sedimentary sources, as well as laterally advected from the southern region of
Heard Island and exchanged through the Polar Front. Similar results were found during KEOPS 1 by
Mongin et al. (2008), Zhang et al. (2008), and Maraldi et al. (2009).

6 Iron fertilization in the KPR has in influence on phytoplankton growth and primary production (PP), and 7 other microbial activities (Cavagna et al., 2014; Christaki et al., 2014), as well as relative CH₄ accumulation (Fig. 3,f and Fig. 4f) and some N_2O depletion (Fig 3e) were also observed. The gas 8 9 distribution pattern clearly matched with TChl-a and PCA grouped stations as was made by Queroue et 10 al (this volume) using dFe. The separation of stations comprises coastal area (Sts. TWE01, -02), PF (St. STWE07) and central plateau region (Sts. A-3). In the case of KEOPS 2, phytoplanktonic blooms 11 were mainly represented by a microplanktonic community (Lasbeiz et al, this volume) as those 12 13 observed in the north Polar Front (St. TWE07) and the central part of the KPR (A3) stations displayed high rates of iron uptake (Quéroué et al, 2014). The mentioned areas, resented variable but high 14 particulate Fe of biogenic origin (van der Merwe et al., 2014), confirming an increased biological 15 uptake, which in turn determines a rapid dFe turnover. The observed gas distribution patterns raise 16 questions as to how the complex circulation and some mesoscale structures support relatively high 17 T*Chl-a* accumulation and microbial activities in comparison to surrounding waters, and particularly 18 whether there are some fertilization mechanisms (including the addition Fe and nutrients) promoting 19 GHG cycling and the concomitant microbial activities. 20

21 **4.2.** N₂O cycling

Fuhrman and Capone (1991) pointed out that stimulating ocean productivity by Fe addition, which
enhances nitrogen export from the euphotic zone to the subsurface layer, can result in enhanced N₂O

1	formation via stimulated nitrification. This stimulation could occur through the activation of
2	metalloproteins that are involved in various steps of ammonium and nitrite oxidation, as ammonia
3	oxidizing nitrifiers use iron-containing ammonia monooxygenase (AMO) and hydroxylamine
4	oxidoreductase (HAO) to oxidize NH_4^+ and NH_2OH , respectively, to NO_2^- (Morel et al, 2003b). Since
5	N ₂ O is a powerful greenhouse gas, 300 times more radiative than CO ₂ per molecule, Fe addition could
6	counteract the climatic benefits of atmospheric CO ₂ drawdown (Jain et al., 2000). The link between Fe
7	fertilization and enhanced N ₂ O formation via nitrification was supported by Law and Ling (2001), who
8	found a small but significant N_2O accumulation in the pycnocline during the Southern Ocean Iron
9	Enrichment Experiment (SOIREE) at 61°S, 140°E. Jin and Gruber (2003) subsequently predicted the
10	long-term effect of Fe fertilization on global oceanic N2O emissions using a coupled physical-
11	biogeochemical model. Based on the model outputs, they concluded that Fe fertilization induced N_2O
12	emissions that could offset the radiative benefits of the CO ₂ drawdown. However, during other Southern
13	Ocean Iron Enrichment Experiments (EIFEX), Walter et al. (2005) found no N ₂ O enrichment after
14	artificial Fe fertilization.
15	Our findings revealed that natural Fe fertilization did not seem to stimulate N_2O accumulation
16	superficially (within the bML). The N_2O inventory estimates from areas of higher accumulation of
17	biomass were not significantly different with respect to those estimated for St. R, which was used as a
18	reference station (Table 2). Contrary to what was expected, no increase in N_2O content was observed at
19	stations close to Kerguelen Island (St TWE01, TWE02), which are highly enriched by dFe from fresh
20	water and sediments (Quéroué et al., this volume). This trend suggests that nitrifiers in surface water are
21	not being significantly stimulated by Fe supply from the sediments. At subsurface water (below ML to
22	500 m depth) N_2O accumulation may be associated to nitrification In fact, dual nitrate isotopic
23	composition (δ^{15} N-NO ₃ ⁻ and δ^{18} O- NO ₃ ⁻) revealed an increasing of values for both isotope values as water

1 depth increase in subsurface waters (100–400 m) as being the result of partial consumption of available nitrate in surface waters, export of low δ^{15} N in Particulate Nitrogen (NP) and remineralisation– 2 nitrification there (Dehairs et al., 2014) Although, values of δ^{15} N-NO₃⁻ and δ^{18} O- NO₃⁻ in surface water 3 also suggested that nitrification is also occurring in surface water, but with a considerable variation 4 Remarkably, the St. TW07-08 and A2-3 were in equilibrium and slightly depleted in N₂O (Fig. 3e; Table 5 6 2). The only plausible explanation is that mixing process produced at the PF (St. TWE07) (which have 7 moderate Fe levels, high T*Chl-a* and evidence of active Fe uptake) may stimulate the N fixers, as 8 demonstrated by Mills et al. (2004), Berman-Frank et al. (2007), and Moore et al. (2009). N-fixing microorganisms may have an effect on the N₂O inventory as they could be used as an alternate substrate 9 10 for fixers, as suggested by Farias et al. (2013). Thus, biological N_2O fixation could be using and assimilating N₂O, producing N₂O depletion and a concomitant undersaturation. N-fixation has been 11 observed in the cold waters of the Arctic and Antarctic (Blais et al., 2012; Diez et al., 2012, Diez 12 unpublished data), as well as in cold upwelled water (Fernandez et al., 2011), suggesting that N_2O 13 fixation may also be action and it is a well-spreading process than originally expected. Coincidently, St. 14 SPF also had the highest surface N-fixation (Gonzalez et al. this volume), suggesting that N₂O is used as 15 a substrate by diazotrophs (Farias et al., 2013) and that this process is stimulated by enhanced Fe supply. 16 N_2O undersaturation or equilibrium with the atmosphere was observed in the N-S transect (Fig. 4e), 17 18 particularly at stations north of the PF bathed by SAMW. This suggests that some process is removing or consuming this gas in the upper water column. A notable level of undersaturation was also observed 19 at St. A3-2, which is located in the recurring phytoplankton bloom and in a regime of relatively high dFe 20 concentración due to the presence of the Plateau (Blain et al., 2007). 21 N₂O undersaturation has been reported, although rarely, in Polar and Sub-polar Ocean regions (Butler et 22

al., 1989; Law and Ling, 2001; Foster et al., 2009). Physical processes related with gas solubility and

1	deviations of from atmospheric equilibrium gas concentration could not explain the observed
2	undersaturation. If these physical variables change in less time than that required for equilibrium of the
3	gases with the atmosphere, there may be a gas deficit. Thus, deviation from the equilibrium condition
4	could be caused by rapid heating or cooling, refreshing, and/or a mixing of water masses (Sarmiento and
5	Gruber, 2006). An analysis of these potential changes was made for the AASW and the SAMW. A
6	cooling (decreasing $T^{\circ}C>3$) or freshening processes (decreasing S from 34 to 10) are required to
7	produce the observed undersaturation, neither of which was observed during the sampling (Table 1), or
8	expected during this season (Park and Viver, 2012). Additionally, if the two water masses were mixed
9	proportionally, as they are, the resulting process cannot produce undersaturation regarding the original
10	N ₂ O levels and their temperature and salinity signature. Recently, Chen et al. (2014) reported that
11	surface water of the Southern Ocean of Indian sector were understaturated in N ₂ O, reflecting also a N ₂ O
12	influx. This phenomenon in the surface water may result from ice melt water intrusion and
13	northeastward transport of the AASW. However, in the KPR, N ₂ O undersaturation seems to be located
14	in area of high particle concentration under the influence if in the SAMW (northern the PF),
15	Thus, a preliminary analysis indicates that biological processes are responsible for the N ₂ O
16	undersaturation and the concomitant influx from the atmosphere. In contrast, subsurface waters have
17	higher N_2O concentrations (saturations from 120% to 180%) than surface waters, which indicate a net
18	accumulation. In this case the plausible process responsible for N_2O accumulation is aerobic ammonium
19	oxidation (Codispoti et al., 2001), but no significant difference was noted at the stations with the highest
20	T <i>Chl-a</i> levels, indicating that N ₂ O production by nitrification was not substantially stimulated at those
21	stations

4.3. CH₄ cycling

1	There have been few studies on CH ₄ distribution and production in the Southern Ocean (Lamontag et al.,
2	1973; Tilbrook and Karl, 1994; Heeschen et al., 2004). There, surface water has been reported to be
3	undesaturated or lightly saturated with respect to atmospheric CH ₄ , as the result from the entrainment of
4	CH ₄ depleted deep water into surface water and from the seasonal ice cover acting as a barrier for gas
5	exchange (Toshida et al., 2011). Regarding the effect of iron addition on CH ₄ cycling Wingenter et al.
6	(2004) found low levels of CH_4 production (less than 1%) during artificial Southern Ocean Fe
7	enrichment experiments (SOFex). Simulated large-scale Southern Ocean Fe fertilization (OIF) also
8	resulted in anoxic conditions which may favor anaerobic methanogenesis (Oschlies et al. 2010).
9	However, our results show that surface and subsurface water are supersaturated in CH ₄ with a fourfold
10	enrichment in CH ₄ with respect to the control area (Fig. 3e), this was associated to areas with elevated
11	T <i>Chl-a</i> levels and iron uptake by microbial communities (Fourquez et al., 2014).). Results showed
12	marked spatial differences in CH ₄ content measured in the W-E and N-S transect (t-student: 3.21
13	p<0.001) (Fig. 3f and 4f), and that surface CH ₄ accumulation generally coincided with areas of relatively
14	higher dFe levels, which in turn favors primary production (PP). Likewise, the CH ₄ accumulation at
15	pycnoclines (Fig. 6) indicates that most CH ₄ came from accumulated particles sinking from the surface
16	water, as commonly observed by Holmes et al. (2000) in different marine systems. The PCA analysis,
17	which included the measurement of dFe revealed a close relationship between CH ₄ accumulation and Fe
18	availability and clearly grouped in areas with different biogeochemical characteristics. The fact that the
19	western and eastern sections showed high Fe levels (Quéroué, this volume) relative to the Central
20	Section of the W-E transect, and that these sections had high CH ₄ levels, suggests that Fe in some way
21	stimulates CH ₄ production. A similar situation occurs in Sts.A3 with high T <i>Chl-a</i> levels and PP rates, as
22	shown by Cavagna et al. (2014). For example, station A3-2 and TWE07 (maximum T <i>Chl-a</i>) had the
23	highest integrated primary production rates (up to 3380 mg $m^{-2} d^{-1}$) and the lowest C export level of

1	around 2-3% (Cavagna et al., 2014), this suggests an intense level of PP supported by regenerated N
2	sources. These contrast with condition found at St. R with the lowest rate of regenerated production
3	(with a PP rate of around 135 mg m ⁻³ d ⁻¹ and an exported C rate of around 25% of PP).
4	Two hypotheses exist about CH ₄ production in surface waters. One is that it should only occur in
5	association with anoxic particles (Karl and Tilbrook, 1994) most of them being produced by grazing
6	zooplankton, as methanogenic bacteria were considered to be present in an anaerobic microenvironment
7	in organic particles (pellets) or in the guts of zooplankton (Alldredge and Cohen, 1987; Karl and
8	Tilbrook, 1994)The other hypothesis was formulated more recently, that that phytoplankton blooms
9	should favor zooplankton grazing process and/or stimulate bacterioplankton activity as CH4 is generated
10	via the degradation of organic methyl compounds by bacteria (Karl et al 2008).
11	Increased grazing of microbes by microzooplankton, as observed by Christaki et al. (2014) and may
12	contribute to particle recycling (rich in organic carbon and DMSP), and increase the potential for
13	methanogenesis (Weller et al., 2013). Yoshida et al. (2011) found that high CH ₄ production in the
14	Southern Ocean probably resulted from the grazing processes of Antarctic krill and/or zooplankton fed
15	on phytoplankton, and the subsequent microbial methanogenesis. This was in line with the findings of
16	iron and biomass enriched sites exhibited the highest carbon fluxes at 100 m depth, mainly dominated
17	by large fecal pellets, rather than phytodetrital aggregates (Laurenceau et al., 2014).
18	On the other hand, aerobic CH_4 production in the water column could be associated with heterotrophic
19	activities. Christaki et al. (2014) showed that the highest bacterial production rates (up to 110 mg C m ^{-2}
20	d ⁻¹), and the greatest abundance of heterotrophic bacteria were associated with stations where the
21	phytoplankton bloom was developed (TWE07 and A3-2). Recent evidences indicate that methylotrophs
22	are candidates for mediated CH_4 generation using methylated compounds as DMSP and DMS (Florez-
23	Leiva et al., 2013; Weller et al., 2013). Among these heterotrophic microorganisms DMS degradation

1 can be ascribed to methylotrophic bacteria (Vissher et al., 1994) that derive energy from the conversion 2 of methyl into other products, as well as using S as a source for methionine biosynthesis (Kiene et al., 3 1999). Current studies of natural and cultivated SAR11 alphaproteobacteria (strain Ca. P. ubique HTCC1062; Sun et al., 2011) indicate that these microorganisms, among the most abundant 4 5 heterotrophic bacteria in surface waters, possess genes that encode for oxidation pathways of a variety of 6 one-carbon compounds, and have the capacity for demethylation and C1 oxidation, but do not incorporate C1 compounds as biomass. These facts suggest a close relationship between phytoplankton, 7 the only producers of DMSP (Yoch, 2002), and microbial communities which may be recycling DMS. 8 9 Phyto-bacterioplankton relationships control DMS turnover, which could result in several mechanisms 10 of DMSP/DMS degradation (Simó et al., 2002; Vila-Costa et al., 2006) and produce CH₄ (Damm et al., 2010; Florez-Leiva et al., 2013; Weller et al., 2013). These authors showed that phytoplankton species 11 composition and biomass in different bloom phases, as well as eddy dynamics, were important 12 determinants of CH₄ saturation and emission. 13 Regarding vertical distribution of this gas, profiles indicate that most CH₄ is being formed at the surface 14 and at pycnoclines (at the base of the ML), and consumed at subsurface and intermediary depths (Figure 15 6). Thus, CH_4 distribution appears to be controlled largely by biological mechanisms rather than by 16

17 mixing, contrary to what has been reported by Heeschen et al., (2004). In general, surface waters of the

18 Southern Ocean were undesaturated with respect to atmospheric CH₄ as the result of the entrainment of

19 CH₄ depleted deep water to the surface and from seasonal ice cover acting as a barrier for gas exchange.

20 We observed CH_4 undersaturation, fluctuating between 40% and 90%, at most sampled stations at

21 depths of > 200. It is unlikely that undersaturation results from the entrainment of CH₄-depleted waters

that have high levels of gas solubility, but also by a biological consumption. It is more likely that a

23 biological mechanism is involved. The only known process able to consume CH₄ is methanotrophy, and

1 the fact that subsurface waters were depleted of CH₄ suggests that CH₄ consumption is higher than 2 production, or that no production occurs in subsurface waters. Interestingly, although CH_4 microbial 3 oxidation occurs throughout the water column and is recognized as an important process that reduces 4 CH_4 emissions (Reeburgh et al., 2007; Rehder et al., 1999), microbial communities mediating aerobic CH₄ oxidation have scarcely been investigated. There have been few measurements of aerobic CH₄ 5 6 oxidation in marine environments, and measurements taken from open systems under oligotrophic regimes (Tilbrook and Karl, 1994, Holmes et al., 2000) have found lower levels of oxidation than in the 7 oxic/anoxic interface (Sansone and Martens, 1978 Reeburgh et al., 1991). 8

9 4.4. CH₄ and N₂O emission in the southern Ocean

Highly dynamic gas exchanges were registered in the KPR, with source and sink scenarios for N₂O and 10 just a source scenario for CH₄. Since the mean wind speed did not exceed 14 m s⁻¹, LM86 and W92 11 parameterizations represent the more conservative overestimation estimates of gas exchange in the area 12 13 (Frost and Upstill-Goddard, 2003). The gas inventories in the ML reflect the effect of gas transport mainly via turbulent mixing and advection, which can be accelerated by the action of wind but also by 14 the microbial activity in surface waters. The ML depth did not correlate to wind speed (rs: 0.31, p< 15 0.05). This fact would explain how much of the content of the gases in the ML may come from in situ 16 17 production or consumption. CH_4 fluxes were higher at stations located at the PF and A3, where phytoplaktonic blooms were observed (see Table 2), but the tendency was the reverse for N₂O, with an 18 influx into the aforementioned stations. CH₄ emission rates during this study were higher than previous 19 measurements (Table 2), with a range of 0.1 to 3.0 μ mol m⁻² d⁻¹ for the Pacific Ocean (Bates et al., 20 1996; Holmes et al., 2000; Sansone et al., 2001) and 0.5 to 9.7 μ mol m⁻² d⁻¹ for the Atlantic Ocean 21 (Oudot et al., 2002; Forster et al., 2009). In the South Pacific ocean (10°-64°S, 140°E), crossing the PF, 22 Yoshida et al. (2011) reported CH₄ fluxes ranging from 2.4 to 4.9 μ mol m⁻² d⁻¹. 23

In the case of N₂O, the estimates in this study were in the expected range for the oligotrophic open ocean
(Nevinson et al., 1995). N₂O undersaturation and a concomitant influx were estimated, although this
situation has not yet been well described for the Southern Ocean. N₂O sinks can occasionally be
observed (Butler et al., 1989; Law and Ling, 2001), the most plausible explanation for which is N₂O
assimilation by N-fixing microorganisms. This process may be responsible for the estimated N₂O influx.

6

7 5. Implications

The dynamics of the both gases differ substantially both spatially and vertically (surface to 500m depth), 8 9 indicating that different mechanisms are being activated producing an active gas during recycling. Our findings also show that in areas of active fertilization and biogenic particle accumulation, CH₄ 10 accumulates while N₂O becomes depleted. This study suggests that the Antarctic Polar Zone plays a 11 significant role in surface CH_4 production and subsequent air-sea gas exchange. These results did not 12 agree with some previous studies of artificial fertilization experiments in the Southern Ocean, even 13 though only a few previous studies exist, indicating that the turnover and evolution of microbial 14 communities in mesoescale structure are fundamental for the development of substrates and conditions 15 for CH_4 regeneration. Surface N₂O does not spatially respond to natural stimulation, at least in terms of 16 17 N_2O production via nitrification or that N_2O consuming are faster than N_2O producing process, but in subsurface water N₂O accumulation seems to take place via nitrification). 18

19

Acknowledgements: We would like to thank the captain and crew of the R/V Marion Dufresne. We are
also grateful to Louise Oriol and Stephane Blain for nutrient data and Marine Lasbleiz for the HPLC
analysis of chlorophyll measurements. We also recognize all our colleagues that contributed to KEOPS
CF and LF were supported by the Proyecto Ecos-Conicyt C09B02 and the International Associated

1	Laboratory MORFUN. CF received partial support from Fondap N°15110027. LF founded the analysis
2	of samples obtained in the KEOPS 2 cruise with FONDECYT N° 1120719. This is a contribution by
3	15110009 (FONDAP-CONICYT).
4 5	References
6 7 8	Alldredge, A. L., and Y. Cohen (1987), Can microscale chemical patches persist in the sea? Microelectrode study of marine snow, fecal pellets, Science, 235, 689–691, doi:10.1126/science.235.4789.689
9 10	Arrieta, J.M., Weinbauer, M.G., Lute, C. and Hernd, G.J. Response of bacterioplankton to iron fertilization in the Southern Ocean, Limnology and Oceanography, 49(3), 799-808, 2004.
11 12	Bates T.B., Kelly, K.C., Johnson, J.E. and Gammon, R.H. A re-evaluation of the open ocean source of methane to the atmosphere, Journal of Geophysical Research, 101 (D3), 6953–6961, 1996.
13 14	Berman-Frank, I. Quigg, A., Finkel Z. V., Irwin A.J., Haramaty, L. Nitrogen-fixation strategies and Fe requirements in cyanobacteria, Limnology and Oceanography, 52(5), 2260–2269, 2007.
15 16 17 18 19 20 21 22	 Blain, S., Quéguiner, B., Armand, L., Belviso, S., Bombled, B., Bopp, L.,Bowie, A., Brunet, C., Brussaard, K., Carlotti, F., Christaki, U., Corbiére, A., Durand, I., Ebersbach, F., Fuda, J.L., Garcia, N., Gerringa, L.J.A., Griffiths, F.B., Guigue, C., Guillerm, C., Jacquet, S., Jeandel, C., Laan, P., Lefe`vre, D., Lomonaco, C., Malits, A., Mosseri, J., Obernosterer, I., Park, Y.H., Picheral, M., Pondaven, P., Remenyi, T., Sandroni, V., Sarthou, G., Savoye, N., Scouarnec, L., Souhault, M., Thuillers, D., Timmermans, K.R., Trull, T., Uitz, J., Van-Beek, P., Veldhuis, M.J.W., Vincent, D., Viollier, E., Vong, L and Wagener, T. Effect of natural iron fertilization on carbon sequestration in the Southern Ocean, Nature, 446 (7139), 1070–1075, 2007.
23 24 25	Blain, S., Sarthou, G. and Laan, P. (2008) Distribution of dissolved iron during the natural iron fertilization experiment KEOPS (Kerguelen Plateau, Southern Ocean), Deep-Sea Research II, doi:10.1016/j.dsr2.2007.12.028, 2008.
26 27 28	Blain, S., Oriol, L., Capparos, J., Gueneugués, A., and Obernosterer, I. Distribution and stoechoimetry of dissolved nitrogen and phosphorus in the iron fertilized region near Kerguelen (Southern Ocean), Biogeosciences discussion KEOPS 2 special issue, 2014.
29 30 31	Blais, M., Tremblay JÉ., Jungblut, A. D, Gagnon, J., Martin, J., Thaler, M. and Lovejoy, C.Nitrogen fixation and identification of potential diazotrophs in the Canadian Arctic. Global Biogeochemical Cycles, 26, GB3022, doi:10.1029/2011GB004096, 2012
32	

Butler, J. H., Elkins, J.W., Thompson, T. M and Egan. K.B. Tropospheric and Dissolved N₂O of the
 West Pacific and East Indian Oceans During the El Niño Southern Oscillation Event of 1987,
 Journal of Geophysical Research, 94, 14865-14877, 1989.

Cavagna, A.J., Lefèvre, D., Dehairs, F., Elskens, M., Fripiat, F., Closset, I., Laslbleiz, M., FlorezLeiva, L., Cardinal, D., Leblanc, K., Fernandez, C, Oriol, L., Blain, S. and Quéguiner, B. Production
regime and potential for carbon export in the naturally iron fertilized Kerguelen area (Southern
Ocean). Biological productivity regime in the surface water around the Kerguelen Island in the
Southern Ocean – from the use of an integrative approach. Biogeosciences discussion KEOPS 2
special issue, 2014.

- Chen. L., Zhang, J., Zhan, L., Li, Y., Sun, H. Differences in nitrous oxide distribution patterns between
 the Bering Sea basin and Indian Sector of the Southern Ocean. Acta Oceanol. 33, P. 9-19, 2014
 DOI: 10.1007/s13131-014-0484-8
- Chever, F., Sarthou, G., Bucciarelli, E., Blain, S. and Bowie, A.R., 2010. An iron budget during the
 natural iron fertilisation experiment KEOPS (Kerguelen Islands, Southern Ocean). Biogeosciences,
 7: 455-468.
- Christaki, U., Lefèvre, D., Georges, C., Colombet, J., Catala, P., Courties, C., Sime-Ngando, T.,
 Blain, S. and Obernosterer, I. Microbial food web dynamics during spring phytoplankton blooms in
 the naturally iron-fertilized Kerguelen area (Southern Ocean), Biogeosciences Discuss, 11, 6985–
 7028, doi:10.5194/bgd-11-6985-2014, 2014.
- Cicerone, R.J. and Oremland, R.S. Biogeochemical aspects of atmospheric methane, Global
 Biogeochemical Cycles, 2, 299–327, 1988.
- Codispoti, L.A and Christensen, J.P. Nitrification, denitrification and nitrous oxide cycling in the eastern
 Tropical South Pacific Ocean, Marine Chemistry, 16, 277-300, 1985.
- Codispoti, L. A., Brandes, J. A. Christensen, J. P. Devol, A.H. Naqvi, S.W.A., Paerl, H.and Yoshinari,
 T. The oceanic fixed nitrogen and nitrous oxide budgets: Moving targets as we enter the
 anthropocene?, Scientia Marina, 65, 85-105, 2001.
- Damm, E., Helmke, E., Thoms, S., Schauer, U., Nöthing, E., Bakker, K., Kiene, R.P. Methane
 production in aerobic oligotrophic surface water in the central Artic ocean, Biogeosciences, 7,
 1099-1108, 2010.
- Dehairs, F, Fripiat, F., Cavagna A.-J. Trull, T. W. Fernandez, C., Davies, , D. Roukaerts A.,
 Fonseca Batista, D. Planchon, F. and Elskens M. Nitrogen cycling in the Southern Ocean
 Kerguelen Plateau area: evidence for significant surface nitrification from nitrate isotopic
 compositions Biogeosciences Discuss., 11, 13905-13955, 2014
- Díez, B., Bergman, B., Pedrós-Alió, C., Antó, M. and Snoeijs P. High cyanobacterial nifH gene
 diversity in Arctic seawater and sea ice brine. Environmental Microbiology Reports 4, 360–366,
 2012 doi:10.1111/j.1758-2229.2012.00343.x

- d'Ovidio, F., Zhou, M., Park, Y. H., Nencioli, F., Resplandy, L., Doglioli, A., Petrenko, A., Blain, S.,
 and Queguiner, B.: Guiding biogeochemical campaigns with high resolution altimetry: waiting for
 the SWOT mission, Proceedings of 20 Years of Progress in Radar. Altimetry Symposium, Venice,
 Italy, 2012.
- Emery, W.J and Thomson, R.E. Data analysis methods in physical oceanography, Pergamon Press, 634
 pp, 1997.
- Farias, L., Fernández, C., Faúndez, J., Cornejo, M. and Alcaman, M.E. Chemolithoautotrophic
 production mediating the cycling of the greenhouses gases N₂O and CH₄ in an upwelling
 ecosystem, Biogeosciences, 6, 3053-3069, 2009.
- Farias, L., Faundez, J., Fernadez, C., Cornejo, M., Sanhueza, S and Carrasco, C. Biological N₂O fixation
 in the eastern South Pacific ocean, PLoS One 8, e63956, doi:10.1371/journal.pome0063956, 2013.
- Florez-Leiva, L., Damm, E. and Farías, L. Methane production induced by methylsulfide in surface
 water of an upwelling ecosystem, Progress in Oceanography, doi.org/10.1016/ j.pocean.
 2013.03.005, 2013.
- Fourquez, M., Obernosterer, I., Davies, D.M., Trull, T.W. and Blain, S. Microbial iron uptake in the naturally fertilized waters in the vicinity of Kerguelen Islands: phytoplankton-bacteria interactions. Biogeosciences Discuss., 11, 15053-15086, 2014
- Frost, T., and Upstill-Goddard, R.C. Meteorological controls of gas exchange at a small English lake,
 Limnol. Oceanogr., 47(4), 2002, 1165–1174, 2002.

Forster, G., Upstill-Goddard, R.C., Gist, N., Robinson, C., Uher, G., Woodward, E.M. Nitrous oxide and
 methane in the Atlantic Ocean between 50°N and 52°S: Latitudinal distribution and sea-to-air flux,
 Deep-Sea Research II 56, 964-976, 2009.

- Fuhrman, J.A. and Capone, D.G. Possible biogeochemical consequences of ocean fertilization,
 Limnology and Oceanography, 36, 1951-1959, 1991.
- Grasshoff, J. Methods of seawater analysis. In: Grasshoff K, Ehrhardt M, Kremling K (eds.). Methods of
 seawater analysis Verlag chimie Germany, 1983.
- Gonzalez, M.L., Molina, V., Florez-Leiva, L. Cavagna, A.J., Dehairs, F., Farias, L. and Fernandez, C.
 Nitrogen fixation in the southern ocean: A case of study of the Fe-fertilized Kerguelen region
 (KEOPS II cruise) MS No.: bg-2014-576
- 29 (KEOPS II Cruise) MIS NO.: 0g-2014-570
- Hanson, R.S. and Hanson, T.E. Methanotrophic bacteria, Microbiology and Molecular Biology
- Reviews, 60(2), 439-471, 1996.
- Heeschen, U. K., Keir, R. S., Rehder, G., Klatt, O and Suess, E. Methane dynamics in the Weddel Sea
 determined via stable isotope ratios and CFC 11, Global Biogeochemical. Cycles, 18, GB2012,
 2004, doi:10.1029/2003GB002151.

- Holmes, R.H., Aminot, A., Kérouel, R., Hooker, B.A., Peterson, J. A simple and precise method for
 measuring ammonium in marine and freshwater ecosystems, Canadian Fisheries and Aquatic
 Sciences, 56:1801-1808, 1999.
- Holmes, M.E., Sansone, F.J., Rust, T.M. and Popp, B.N. Methane production, consumption, and air-sea
 exchange in the open ocean: An evaluation based on carbon isotopic ratios, Global Biogeochemical
 Cycles, 14, 1 10, 2000.
- Hughes, C.W. Rossby waves in the southern ocean: A comparison of TOPEX/POSEIDON altimetry
 with model predictions, Journal Geophysical Research, 100, 15933–15950, 1995.
- Hughes, C.W. The Antarctic Circumpolar Current as a waveguide for Rossby waves, Journal Physical
 Oceanography, 26, 1375–1387, 1996.
- IPCC. Climate Change: The Physical Science Basis: Working Group I Contribution to the Fourth
 Assessment Report of the IPCC (Climate Change 2007), M. Tignor and H.L. Miller [eds.].
 Cambridge University Press, 2007.
- Jain, A. K., Briegleb, B.P., Minschwaner, K. and Wuebbles D. J. Radiative forcing and global
 warming potentials of 39 greenhouse gases, Journal Geophysical Research, 105, 20,773–20,790.,
 2000.
- Jin, X. and Gruber, N. Offsetting the radiative benefit of ocean iron fertilization by enhancing N₂O
 emissions. Journal Geophysical Research, 30, NO. 24, 2249, doi:10.1029/2003GL018458, 2003.
- Jickells, T. D., An, Z. S., Andersen, K. K., Baker, A. R., Bergametti, G., Brooks, N., Cao, J. J., Boyd, P.
 W., Duce, R. A., Hunter, K. A., Kawahata, H., Kubilay, N., laRoche, J., Liss, P. S., Mahowald, N.,
 Prospero, J. M., Ridgwell, A. J., Tegen, I., and Torres, R.: Global iron connections between desert
 dust, ocean biogeochemistry, and climate, Science, 308, 67-71, 2005
- Jouandet, M-P., Jackson, G. A., Carlotti, F., Picheral, M.,Stemmann, L. and Blain, S. Rapid formation
 of large aggregates during the spring bloom of Kerguelen Island: observations and model
 comparisons Biogeosciences Discuss., 11, 4949–4993, doi:10.5194/bgd-11-4949-2014, 2014.
- Karl, D.M., Tilbrook, B.D. Production and transport of methane in oceanic particulate matter, Nature,
 368, 732–734, 1994.
- Karl, D., Beversdorf, L., Björkman, K.M., Church, M.J., Martinez, A., DeLong, E.F. Aerobic production
 of methane in the sea, Nature Geoscience, 1, 473-478, 2008.
- Kiene, R.P. Linn, L.J. J. Gonzalez, J. M.A. Moran, M.A Bruton, J.A. Dimethylsulfoniopropionate and
 methanethiol are important precursors of methionine and protein-sulfur in marine bacterioplankton.
 Applied and Environmental Microbiology, 65 (10),4549–4558, 1999.

Kirchman, D.I, Hoffman, K.A. Weaver, R. and Hutchins, D.A. Regulation of growth and energetics of a
 marine bacterium by nitrogen source and iron availability, Marine Ecology Progress Series, 250,
 291-296, 2003.

Laurenceau, E.C., Trull, T. W., Davies, D. M., Bray, S. G., Doran, J., Planchon F., Carlotti, F.,
Jouandet, M.-P., Cavagna, A.-J., Waite, A. M. and Blain S. The relative importance of
phytoplankton aggregates and zooplankton fecal pellets to carbon export: insights from free-drifting
sediment trap deployments in naturally iron-fertilised waters near the Kerguelen plateau.
Biogeosciences Discuss., 11, 13623-13673, 2014. doi:10.5194/bgd-11-13623-2014

- Law, C. and Ling, R. Nitrous oxide flux and response to increased iron availability in the Antarctic
 Circumpolar Current, Deep Sea Research Part II: Topical Studies in Oceanography, 48, 2509-2527,
 2001.
- Lasbleiz, M., Leblanc, K., Blain, S., Ras, J., Cornet-Barthaux, V., Nunige, S.H. and Quéguiner, B.,
 2014a. Pigments, elemental composition (C, N, P, Si) and stoichiometry of particulate matter, in the
 naturally iron fertilized region of Kerguelen in the Southern Ocean. Biogeosciences Discuss., 11:
 8259–8324, doi:10.5194/bgd-11-8259-2014.
- Liss P.S, Merlivat L. Air-sea gas exchange rates: Introduction and synthesis. In: Buat-Menard P. (ed.),
 The Role of Air-Sea Exchange in Geochemical Cycling. D. Reidel, Dordrecht, pp. 113-127, 1986.
- Nevison, C., Weiss, R. and Erickson III, D.J. Global oceanic emissions of nitrous oxide, Journal of
 Geophysical Research, 100, 15809-15820,1995.
- Nevison, C., Butler, J.H. and Elkins, J.W. Global distribution of N₂O and the DN2O-AOU yield in the
 subsurface ocean, Global Biogeochemical Cycles, 7 (4), 1119, doi:10.1029/2003GB002068, 2003.
- Maraldi, C., Mongin, M., Coleman, R.S. and Testut, L. The influence of lateral mixing on a
 phytoplankton bloom: distribution in the Kerguelen Plateau region. Deep Sea Research Part I, 56:
 963-97, 2009.
- Mills, M.M.,Ridame, C., Davey, M., La Roche, J and Geider, R. Iron and phosphorus co-limit nitrogen
 fixation in the eastern tropical North Atlantic, Nature., 429, 292–294, 2004.

Mongin, M., Molina, E. and Trull, T. Seasonality and scale of the Kerguelen plateau phytoplankton
bloom: A remote sensing and modeling analysis of the influence of natural iron fertilization in the
Southern Ocean, Deep Sea Research Part II: Topical Studies in Oceanography, 55(5-7), 880-892,
2008.

Moore, C.M , Mills, M.M., Achterberg, E.P., Geider., R J. LaRoche, J., Lucas, MI., McDonagh, E.L.,
Pan, X., Poulton, A.J., Rijkenberg, M J. A., Suggett, D.J., Ussher, S. J. and Woodward, E.M.S.
Large-scale distribution of Atlantic nitrogen fixation controlled by iron availability, Nature
Geoscience, 2, 867–871, 2009.

Morel, F.M.M. and Price, N.M. The biogeochemical cycles of trace metals in the Oceans, Science, 300,
 944, DOI: 10.1126/science.1083545, 2003a.

Morel, F. M. M., Milligan, A.J. and Saito M.A.. Marine Bioinorganic Chemistry: The Role of Trace of
 Metals in the Oceanic Cycles of Major Nutrients in *Treatise on Geochemistry*, Vol. 6, edited by
 KK. Turekian, H.D. Holland, Elsevier Science Ltd, Cambridge, UK, p. 113-143, 2003b

- Oudot, C., Jean-Baptiste, P., E. Fourreb, E. Mormichea, C. Guevela, M., Ternonc, J.-F, Le Corred, P.
 Transatlantic equatorial distribution of nitrous oxide and methane, Deep-Sea Research I, 49,1175–
 1193, 2002.
- Oschlies, A., W. Koeve W., Rickels W., and Rehdanz, K. Side effects and accounting aspects of
 hypothetical large-scale Southern Ocean iron fertilization, Biogeosciences 7, 4017–4035, 2010.
- Park, Y-H and Viver, F. Circulation and hydrography over the Kerguelen Plateau. Marine ecosystems
 and fisheries, 5,43-55, 2012.

Park, Y.-H., Durand, I., Kestenare, E., Rougier, G., Zhou, M., d'Ovidio, F., Cotté, C. and Lee, J.-H.
 Polar Front around the Kerguelen Islands: An up-to-date determination and associated circulation of surface/subsurface waters. J. Geophys. Res. Oceans, 119: doi:10.1002/2014JC010061, 2014.

- Patterson, S L. Surface Circulation and Kinetic Energy Distributions in the Southern Hemisphere
 Oceans from FGGE Drifting Buoys, Journal of Physical Oceanography, 15, 865–884, 2005.
- Quéroué, F., Sarthou, G., Chever, F., van der Merwe, P., Lannuzel, D., Townsend, A.,Bucciarelli, E,
 Planquette, H., Cheize, M., Blain, d'Ovidio, F. and A. Bowie, A. A new study of natural Fe
 fertilization processes in the 2 vicinity of the Kerguelen Islands (KEOPS 2 experiment), KEOPS 2
 special issue (in preparation).
- Rees, A.P., Owens, N.J.P and Upstill-Goddard, R.C. Nitrous oxide in the Bellingshausen Sea and Drake
 Passage, Journal of Geophysical Research, 102, 3383–3391, 1999.
- Reeburgh, W.S, Ward, B.B, Whalen, S.C., Sandbeck, K.A., Kilpatrick, L.J and Kerkhof, K. Black Sea
 methane geochemistry, Deep-Sea Research II (38) S1189–S1210, 1991.
- 26 Reeburgh, W.S. Oceanic methane biogeochemistry, Chemical Reviews 107, 486–513, 2007.
- Rehder, G., Keir, R.S., Suess, E., Rhein, M. Methane in the northern Atlantic controlled by microbial
 oxidation and atmospheric history, Geophysical Research Letters 26, 587–590, 1999.
- Rhee, T. S., Kettle, A. J and Andreae, M. O. Methane and nitrous oxide emissions from the ocean: A
 reassessment using basin-wide observations in the Atlantic, Journal of Geophysical Research,
 114,D12304, doi:10.1029/2008JD011662, 2009.
- Sanial, V., van Beek, P., Lansard, B., Souhaut, M., Kestenare, E., and d'Ovidio, F.: Radium isotopes to
 track sediments-derived inputs of the Kerguelen Plateau, Biogeosciences, Biogeosciences

Discuss., 11, 14023-14061, 2014 Sandwell, D.T, and Zhang, B. Global mesoscale variability from 1 2 the Geosat exact repeat mission: Correlation with ocean depth, Journal of Geophysical Research, 94, 17, 971–17,984, doi:10.1029/JC094iC12p17971, 1989. 3 Sansone F.J. and Martens, C.S. Methane oxidation in Cape Lookout Bight, North Carolina, Limnology 4 and Oceanography, 23, 349-355, 1978. 5 Sansone, F.J., Popp, B.N., Gasc, A. Graham, W. Rust, T.M. Highly elevated methane in the eastern 6 tropical North Pacific and associated isotopically enriched fluxes to the atmosphere, Geophysical 7 Research Letters, 28 4567-4570, 2001. 8 9 Sarmiento, J.L. and Gruber, N. Ocean Biogeochemical Dynamics. Princeton University Press, 2006. 10 Scranton, M.I and Brewer, P. Occurrence of methane in the near-surface waters of the western subtropical North Atlantic, Deep-Sea Research, 24, 127-138, 1977. 11 Simó, R., Archer, S.D., Pedró-Alió, C., Gilpin, L., Stelfox-Widdicombe, C.E. Coupled dynamics of 12 dimethyl- sulfoniopropionate and dimethylsulfide cycling and the microbial food web in surface 13 waters of the North Atlantic, Limnology and Oceanography, 47, 53-61, 2002. 14 15 Sun, J., Steindler, L. J. Thrash, C., Halsey, K.H., Smith, D.P. Amy E. Carter, A.E., Zachary C. Landry, Stephen J. Giovannoni. One Carbon Metabolism in SAR11 Pelagic Marine Bacteria. PloS 16 one DOI: 10.1371/journal.pone.0023973, 2011. 17 18 Tilbrook, E.D and Karl, D.M. Dissolved methane distributions, sources, and sinks in the western Bransfield Strait, Antarctica, Journal of Geophysical Research, 99, 16383–16393, 1994. 19 Tréguer P, Le Corre P Manuel d'analyse des sels nutritifs dans I'eau de mer Uti:lisation de 20 21 1'AutoAnalyzt-r 2 Technicon, 2nd edn. 'Univ Bretagne occidentale, Brest, 1975. Turner, S.M., Harvey, M. J., Law, C. S., Nightingale, P.D and Liss P.S. Iron-induced changes in oceanic 22 sulfur biogeochemistry, Geophysical Research Letter, 31, L14307, doi:10.1029/2004GL020296, 23 2004. 24 van der Merwe, P., Bowie, A.R., Quéroué, F., Armand, L., Blain, S., Chever, F., Davies, D., Dehairs, F., 25 Planchon, F., Sarthou, G. et al., 2014. Sourcing the iron in the naturally-fertilised bloom around the 26 Kerguelen Plateau: particulate trace metal dynamics Biogeosciences Discuss., 11: 13389–13432, 27 doi:10.5194/bgd-11-13389-2014. 28 29 Vila-Costa, M., Simó, R., Harada, H., Gasol, J.M., Slezak D. and Kiene, R.P. Dimethylsulfoniopropinate uptake by marine phytoplankton, Science, 314, 652, 2006. 30 Vissher, P.T., Kiene, R.P., Taylor B.F. Demethylation and cleavage of demethylsulfoniopropionate in 31 marine intertidal sediments, FEMS Microbiology Ecology, 14 179-190, 1994. 32

Walter, S., Peeken, I., Lochte, K and Bange, H.W. Nitrous oxide measurements during EIFEX, the
 European Iron Fertilisation Experiment in the subpolar South Atlantic Ocean, Geophysical
 Research Letter, 32, L23613,doi: 10.1029/2005GL024619, 2005.

Wingenter, O.W., Haase, K.B., Strutton, P., Friedrich, G., Meinardi, S., Blake, D.R and Rowland, F. S.
Changing concentrations of CO, CH₄, C₅H8, CH₃Bt, CH₃I and dimethyl sulfide during the Southern
Ocean Iron Enrichment Experiments, Proceedings of the National Academy of Sciences101, 8537–
8541, 2004.

- Wanninkhof, R. Relationship between wind speed and gas exchange over the ocean, Journal
 Geophysical Research, 97, 7373-7382, 1992.
- Weisenburg, D.A and Guinasso, N.L. Equilibrium solubilities of methane, carbon monoxide and
 hydrogen in water and seawater, Journal of Chemical Engineering Data, 24, 354-360, 1979.
- Weiss, R.F. and Prince, B. A. Nitrous oxide solubility in water and seawater, Marine Chemistry 8, 347 359, 1980.

Weller D.I., Law, C.S., A. Marriner, A., Nodder S.D., Chang, F.H., Stephens, J.A., Wilhelm S.W.,
Boyd P.W., Sutton P.J.H. Temporal variation of dissolved methane in a subtropical mesoscale
eddy during a phytoplankton bloom in the southwest Pacific Ocean, Progress in Oceanography.,
116, 193–206, 2013.

- 18 Wolfe, R.S. Microbial formation of methane, Advance Microbial Physiology, 6, 107–146, 1971.
- Wuebbles, D.J and Hayhoe, K. Atmospheric methane and global change, Earth-Science Reviews, 57,
 177–210, 2002.
- Yoch, D. Dimethylsulfoniopropionate: Its Sources, Role in the Marine Food Web, and Biological
 Degradation to Dimethylsulfide Appl Environ Microbiol. Dec 2002; 68(12): 5804–5815, 2002.
 doi: 10.1128/AEM.68.12.5804-5815.2002
- Yoshida, O., Inoue,H. Y., Watanabe, S, Suzuki, K. and Noriki, S. Dissolved methane distribution in
 the South Pacific and the Southern Ocean in austral summer J. Geophysical Research 116, C07008,
 2011, doi:10.1029/2009JC006089, 2011
- Zhang, Y., Lacan, F. and Jeandel, C. Dissolved rare earth elements tracing lithogenic inputs over the
 Kerguelen Plateau (Southern Ocean), Deep Sea Research Part II: Topical Studies in Oceanography,
 55(5-7): 638, 2008.
- Zhou, M., Zhu, Y., d'Ovidio, F., Park, Y.-H., Durand, I., Kestenare, E., Sanial, V., Van-Beek, P.,
 Queguiner, B., Carlotti, F., and Blain, S.: Surface currents and upwelling in Kerguelen Plateau
 regions, Biogeosciences Discuss., 11, 6845–6876, 2014.
- 33

34

1

3

7

2 Figure caption

Figure 1. Map showing the location of biogeochemical stations sampled during the KEOPS 2 cruise.
Bathymetric topography is shown in the main oceanographic region. The orange line delimits the

6 position of the polar front. The sampled transects are indicated.

Figure 2. Left column: a)Temperature (T°C), c)Salinity and e) T-S diagram for W-E transect. Station
located under the influence of PFZ (purple) is shown, showing enhanced water mass mixing. Arrows
indicate position of PF crossing this transect. Right column:b)Temperature(T°C), d) Salinity and f) T-S
diagram for W-E transect.

12

Figure 3. Vertical cross section of a) nitrate (μ mol L⁻¹); b) phosphate (μ mol L⁻¹); c) chlorophyll-a (μ g L⁻¹); d) dissolved oxygen (μ mol L⁻¹), e) nitrous oxide (nmol L⁻¹) and f) methane (nmol L⁻¹) for for zonal transect between 69-75°E. Arrows indicate position of PF crossing this transect

- Figure 4. Vertical cross section of a) nitrate (μmol L⁻¹); b) phosphate (μmol L⁻¹); c) chlorophyll-a (μg
 L⁻¹); d) dissolved oxygen (μmol L⁻¹), e) nitrous oxide (nmol L⁻¹); f) methane (nmol L⁻¹) for the
 meridional transect between 45°-51°S.
- 20

Figure 5. PCA analysis with environmental data including dissolved iron obtained in zonal transect (TWE). PCA comprises a) data from the surface to the ML's base and b) environmental data from the surface to 500 m depth. Each station along with the eigenvectors are included.

24

Figure 6. Vertical distribution of biogeochemical variables from selected stations with particular
oceanographic and biogeochemical characteristics. Different biogeochemical regimes are defined as
HNLC area (St. R), northern and southern area of Polar front (St. NS01 and A3) and within the Polar

- 28 front (Sts. TWE03 and TWE07)
- 29
- 30

Biogeochemical Provinces	Stations	Latitude	Longitude	Date	Bottom Depth	MLD	Temperature	Salinity	Oxygen
1 i ovinces		°E	°S	mm-dd- yy	(m)	(m)	(°C)		(µmol/Kg)
	OISO-6	-44.59	52.06	10-15-11	3260	110	3.68 (3.66-3.68)	33.80 (33.80-33.81)	317.4 (314-318)
	OISO-7	-47-4	58.00	10-16-11	4300	127	4.75 (4.73-4.76)	33.79 (33.8-33.81)	308.4 (305-309)
N-S transect									
	A3-1	-50,38	72.05	10-19-11	535	181	1.68 (1.68-1.73)	33.89 (33.85-33.91)	325.9 (321-327)
	A3-2	-50.38	72.05	10-16-11	527	165	2.16 (2.10-2.18)	33.91 (33.911- 33.913)	333.2 (329-335)
	TNS10	-50.12	72.07	10-21-11	565	163	1.67 (1.59-1.68)	33.90 (33.80-33.93)	325.9 (314-327)
Eddy	TNS09	-49.47	72.12	10-21-11	615	137	1.75(1.66-1.89)	33.91(33.80-33.84)	321.1 (265-331
Eddy	TNS08	-49.27	72.14	10-21-11	1030	139	2.11 (2.06-2.12)	33.869 (33.86-33.87)	329.4 (324-328
	TNS07	-49.08	72.17	10-22-11	1890	62	2.10 (1.95-2.16)	33.86 (33.86-33.87)	327.7 (327-331
	TNS06	-48.48	71.18	10-22-11	1885	67	2.32 (2.23-2.42)	33.846 (33.84-33.85)	327.6 (315-316
	TNSO5	-48.28	72.12	10-22-11	2060	114	2.22 (2.09-2.26)	33.85 (33.85-33.86)	326.7(323-328
	TNS03	-47.05	71.55	10-23-11	540	111	2.17 (2.06-2.26)	33.89(33.88-33.89)	307.6(304-310
	TNS02	-47.19	71.42	10-23-11	520	65	3.60 (3.38-3.67)	33.69 (33.68-33.69)	318.6 (317-319
	TNS01	-46,.49	71.30	10-23-11	2280	45	4.02(3.96 - 4.13)	33.71(33.71-33.72)	316.1 (315-318
HNLC	RK2-2	-50.21	66.43	10-23-11	2300	111	2.11 (2.06-2.14)	33.78 (33.77-33.78)	326.7 (326-327
E-W transect									
(Shelf)	TEW1	-49,08	69.50	10-31-11	86	16	3.27 (3.17-3.36)	33.61(33.61-33.62)	344.16 (340-34
(Shelf)	TEW2	-48,53	70.39	10-31-11	84	40	2.55 (2.49-2.68)	33.75 (33.75-33.76)	332,0 (327-337
(Shelf)	TEW3	-48,47	71.01	10-31-11	565	62	2.17 (2.12-2.31)	33.86 (33.86-33.87)	329.69 (328-33
(NPF)	TEW4	-48,37	71.28	11-01-11	1585	95	2.54 (2.41-2.60)	33.85 (33.85-33.86)	334.60 (331-33
	TEW5	-48,28	72.47	11-01-11	2275	60	2.51 (2.39-2.60)	33.84 (33.84-33.85)	331.42 (327-33)
(SPF)	TEW7	-48,27	73.59	11-02-11	2510	17	4.02 (3.91-4.10)	33.78 (33.784-33.79)	315.95 (346-349
	TEW8	-48,28	75.19	11-02-11	2786	22	4.15 (4.08-4.18)	33.76 (33.76-33.77)	338.75(347-350
Time Series Stations									
	E1-1	-48.27	72.11	10-28-11	2056	84	2.48 (2.36-2.54)	33.85(33.84-33.85)	331.54(328-333
	E1-2	-48.31	72.04	11-01-11	2003	42	2.42 (2.28-2.56)	33.85 (33.85-33.86)	331.68 (329-333
	E1-3	-48.41	71.58	11-03-11	1915	41	2.74 (2.60-2.81)	33.84 (33.84-33.85)	332.08 (331-332
	E1-4W	-48.45	71.25	11-11-11	1384	67	2.36 (2.07-2.51)	33.90 (33.90-33.91)	329.95 (326-332
	E1-4E	-48.42	72.33	11-12-11	2210	77 26	3.15 (2.78-3.19)	33.84 (33.83-33.85)	329.89 (326-33)
	E1-5	-48.24	71.50	11-18-11	1920	36	2.53 (2.50-2.62)	33.85 (33.85-33.85)	326.97(330-333

Table 1. General oceanographic features of the sampled stations during the KEOPS 2 cruise

												Wind	Flux	LM86	Flux	W92
Station	Inventory in the MLD		Inventory in the Water Column			GHGs										
	*Chl-a	CH ₄	N ₂ O	NO ₃ .	PO4 ³⁻	N ₂ O	CH ₄	NO ₃ -	PO4 ³⁻	N ₂ O	CH ₄		N ₂ O	CH ₄	N ₂ O	CH ₄
	mg m ⁻²	mmol m ⁻²	mmol m ⁻²	mol m ⁻²	mol m ⁻²	mmol m ⁻²	mmol m ⁻²	mol m ⁻²	mol m ⁻²	nM	nM	m s ⁻¹	μmol	m ⁻² d ⁻¹	µmol	m ⁻² d ⁻¹
N-S Transect																
A3-1	12.60	3.00	2.43	5.41	0.293	5.72	4.12	7.342	0.940	13.73	6.56	6.58	-1.54	18,75	-2.96	35.93
A3-2	35.48	3.31	1.81	4.38	0.300	5.273	3.31	15.04	1.024	11.64	8,,37	11.39	-10.5	14.24	-22.9	29.70
TNS10	14.09	1.39	2.56	4.79	0.319	9.29	2.17	16.03	1.077	15.49	7.79	12.66	3.57	14.90	6.56	27.48
TNS09	35.58	1.33	2.23	3.91	0.254	7.51	1.87	12.53	0.864	15.89	14.54	14.38	5.08	38.10	9.36	70.26
TNS08	23.23	0.68	2.16	3.98	0.260	9.27	1.58	15.75	1.038	15.46	5.65	11.89	4.29	7.80	7.92	14.38
TNS07	25.45	0.25	1.02	1.69	0.111	9.99	1.80	15.74	1.072	16.92	4.01	11.89	8.65	2.03	15.55	3.66
TNS06	16.33	0.57	0.92	1.83	0.123	8.65	2.54	15.93	1.070	13.81	8.74	11.89	-0.78	17.59	-1.20	31.64
TNSO5	17.19	0.74	1.68	3.07	0.212	9.27	2.46	15.39	1.070	14.67	6.41	11.40	1.81	9.91	3.26	17.82
TNS03	17.28	0.88	1.75	3.06	0.214	7.75	3.14	12.46	0.875	11.05	7.23	11.40	4.13	9.93	6.85	16.44
TNS02	11.25	0.26	0.91	1.73	0.123	8.27	1.57	15.08	1.046	13.92	4.38	9.73	1.48	3.03	2.45	5.00
TNS1	11.21	0.39	0.63	1.07	0.076	8.89	3.16	14.17	0.976	13.95	8.48	9.73	2.26	14.40	3.74	23.84
RK2-2	14.89	0.64	1.63	2.79	0.197	2.83	1.06	4.900	0.347	14.83	6.29	6.86	0.89	4.09	1.34	6.15
W-E Transect																
TEW1	9.78	0.19	0.26	3.40	0.412	1.18	1.30	1.560	0.111	15.29	9.50	4.60	0.87	3.15	1.69	6.15
TEW2	9.87	0.43	0.62	0.84	1.073	1.12	1.74	1.873	0.133	15.03	9.88	4.60	0.54	3.24	1.06	6.33
TEW3	8.77	0.73	0.91	0.51	1.566	7.41	2.40	14.97	1.072	15.56	14.09	4.60	0.67	5.25	1.32	10.24
E1-2	15.33	0.52	0.20	0.82	1.167	9.78	2.80	15.24	1.051	14.95	11.42	6.92	1.34	11.67	2.01	17.57
TEW4	35.53	0.40	1.63	0.30	2.468	10.3	1.81	15.74	1.106	16.62	3.50	6.92	3.76	0.21	5.67	0.32
TEW5	23.11	0.38	0.99	0.52	1.619	10.21	2.61	15.62	1.099	16.31	6.35	6.92	3.28	4.34	4.94	6.54
TEW7	75.45	0.19	0.23	2.39	0.353	9.26	7.44	15.23	1.087	12.90	10.87	8.04	-0.96	15.42	-1.52	23.78
TEW8	59.52	0.10	0.37	1.52	0.472	10.05	1.59	15.27	1.058	15.77	4.95	8.04	5.25	3.52	8.10	5.42

Table 2. Inventories of gases and nutrients estimated in the mixed layer (ML) and the entire water column, along with GHG concentrations, wind velocities and concomitant estimated gas exchange across the air-sea interface

*Inventories estimated from the photic zone